Predictive modeling of PMMA-based polymer composites reinforced with hydroxyapatite: a machine learning and FEM approach

Rohit Kumar Singh, Khyati Verma, G. C. Mohan Kumar
Department of Mechanical Engineering, National Institute of Technology Karnataka, India
rohitking1007@gmail.com, https://orcid.org/0009-0002-0387-0389
kverma@nitk.edu.in, https://orcid.org/0000-0001-5912-3572
mkumargc@nitk.edu.in, https://orcid.org/0000-0002-7282-7512

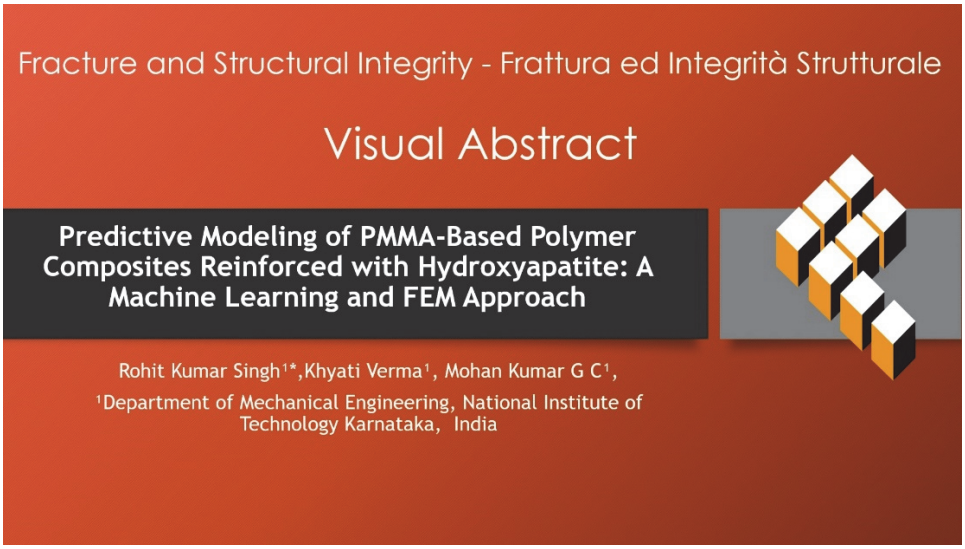

Citation: Singh, R. K., Verma, K., Kumar, G C. M., Predictive modeling of PMMA-based polymer composites reinforced with hydroxyapatite: a machine learning and FEM approach, Fracture and Structural Integrity, 73 (2025) 74-87.

Received: 21.03.2025
Accepted: 30.04.2025
Published: 07.05.2025
Issue: 07.2025

KEYWORDS. Multiscale modeling, RVE, PMMA, Hydroxyapatite (HAp), Polymer matrix composites, Machine learning

INTRODUCTION

Polymer-based composite materials (PMCs) are highly durable high-performance engineering materials that are gaining popularity across a range of industries due to their many beneficial characteristics and immense usability. Their low heat conductivity 0.2–0.5 W/m·K, easy fabrication, corrosion resistance, and high strength-to-weight ratio make them suitable for use in biomedical, automotive, aerospace, and other technological industries [1-3]. Two major classes of PMCs can be indicated: thermoset and thermoplastic polymers. Thermoset materials provide sturdiness and lifetime performance but do not allow any reheating or remolding once formed due to irreversible chemical changes. Thermoplastic polymers such as PMMA can be reheated, remolded and cooled without affecting its chemical properties which can be used in multiple applications [4]. Polymethyl methacrylate (PMMA) is widely utilized in biomedical applications, including bone cement and dental prosthetics, due to its biocompatibility and ease of processing. However, PMMA exhibits poor osseointegration, and non-degradability, which can impede effective bone regeneration and integration with host tissues.

Additionally, PMMA's high exothermic polymerization temperature poses risk of thermal necrosis to surrounding tissues, and the potential release of toxic monomers. To address these challenges, incorporating hydroxyapatite (HAp) into PMMA matrices has been explored, aiming to enhance boicompatibility and mechanical properties to improve osseointegration and overall performance in orthopedic and dental applications. Hydroxyapatite (HAp) is utilized within this context for improvement purposes due to its natural occurrence and calcium apatite composition which closely resembles human bone and teeth. Hydroxyapatite is available from naturally as well as artificially synthesized sources. The natural sources of hydroxyapatite from animal bones are subjected to treatments to extract pure HAp by deproteinizing and calcining under high temperatures. Some synthetic methods are used for producing HAp include wet chemical precipitation, sol-gel processes, and hydrothermal techniques. The process of synthesis basically involves controlled reactions between sources of calcium and phosphate to form HAp crystals, which can be synthesized in accordance to particle size, crystallinity, and morphology, towards the maximization of mechanical reinforcement of the PMMA matrix. Elastic Modulus and Compressive Strength are critical performance indicators that directly influence the structural integrity and functional effectiveness of PMMA-HAp composites. As regards biocompatibility, HAp increases biocompatibility and osteoconductivity; hence, it can promote bone growth, making it ideal for areas of application such as dental implants, bone grafts as well as other load-bearing biomedical devices. HAp will not only augment the mechanical properties of the PMMA matrix, but will also increase its biocompatibility, facilitating better performance concerning biological tissues [5]. Electrospun PMMA/nHA nanofibrous scaffolds have shown enhanced osteoconductivity, improved thermal stability, and excellent biocompatibility for bone tissue engineering applications. The incorporation of nHA improved scaffold morphology and mechanical properties, promoting osteoblast attachment and proliferation, as confirmed by SEM-EDS, FTIR, and biological studies [6]. Kevlar/glass fabric-reinforced epoxy composites were optimized for mechanical properties, with phosphoric acid treatment improving Kevlar composites' Young's modulus by 38%. Additionally, a novel PMMA/hydroxyapatite/$ZnFe_2O_4$/ZnO composite demonstrated excellent antimicrobial activity (zone value) and biocompatibility, showing strong potential for 3D-printed biomedical implants [7] [8]. Nanodiamonds (NDs) have been shown to enhance the stiffness and strength of polymer matrices, with studies reporting up to an 18.5% increase in Young's modulus and a 45.3% rise in hardness for HDPE reinforced with 0.1 wt% NDs [9]. Similarly, incorporating HAp nanoparticles into PMMA matrices improves stiffness and strength by acting as stress-transfer agents, making it promising for biomedical applications. However, predicting the elastic modulus of PMMA-HAp composites remains challenging due to complex interactions at different scales, highlighting the need for advanced modeling techniques to capture these non-linear behaviors accurately. To address these limitations, this study adopts an integrated approach combining experimental testing, Representative Volume Elements (RVE)-based micromechanical modeling, and machine learning (ML) techniques, including Feedforward Neural Network (FFNN), Radial Basis Neural Network (RBNN), and Support Vector Machine (SVM), to predict the Elastic Modulus and Compressive Strength of PMMA-HAp composites [10-11].In recent years, machine learning (ML) has emerged as a powerful tool in materials science, offering advanced methods for predicting and optimizing the mechanical properties of composite materials. ML algorithms can analyze complex, non-linear relationships between compositional variables and material properties, facilitating the design of composites with tailored characteristics. This study advances the prediction of Elastic Modulus and Compressive Strength in PMMA-HAp composites by integrating experimental methods, RVE-based micromechanical modeling, and machine learning (ML) techniques. Compared to Meddage et al. [12], who used ML to predict compressive strength in graphene oxide/cement composites but lacked microstructural modeling. This study provides a more comprehensive understanding of agglomeration and interphase behavior. Similarly, while Yang et al. [13] effectively applied ML for CNT/cement composites considering size effects but their approach did not incorporate detailed microstructural interactions. This approach enhances predictive accuracy and generalization by leveraging RVE models to account for microstructural complexities, while ML algorithms capture non-linear interactions between compositional variables and mechanical properties. The integrated framework enables virtual prototyping, reduces the need for extensive physical experiments, and optimizes material design by exploring a wider range of composite configurations. Moreover, it provides a comprehensive understanding of structure-property relationships by simulating realistic microstructures and identifying complex dependencies between microstructural parameters and mechanical outputs. SVM consistently delivered robust predictions closely aligning with both experimental and theoretical results, demonstrating the efficacy of this hybrid approach. By combining empirical validation with theoretical predictions and advanced predictive modeling, this study overcomes the limitations of traditional methods, offering high predictive accuracy, enhanced generalization, and valuable insights for optimizing composite designs [14]. Traditional models, such as Voigt and Reuss bounds, provide theoretical estimates for Elastic Modulus and Compressive Strength but fail to account for complex microstructural interactions in PMMA-HAp composites, including agglomeration effects and interphase behavior. Previous studies have used homogenization techniques and finite element models but often assume uniform particle dispersion and perfect bonding, leading to inaccuracies, particularly at higher HAp concentrations. This study

advances the field by integrating Representative Volume Element (RVE) micromechanical modeling with machine learning (ML) algorithms to address these limitations more effectively. Unlike earlier models, the RVE approach explicitly simulates heterogeneous particle distributions, including agglomerates, providing a realistic representation of microstructure. Additionally, the model incorporates interphase behavior by simulating the gradient in mechanical properties from the HAp particle to the PMMA matrix, capturing stress transfer mechanisms more accurately. The use of ML algorithms, particularly Support Vector Machines (SVM), further enhances predictive accuracy by identifying complex non-linear interactions between microstructural features and mechanical properties. This integrated methodology not only improves prediction accuracy but also offers deeper insights into the structure-property relationships of PMMA-HAp composites, paving the way for optimized material design and application

MATERIALS AND METHODS

This study integrates a Representative Volume Element (RVE)-based finite element method with experimental validation and machine learning models (FFNN, RBNN, SVM) to evaluate and predict the elastic properties of PMMA-HAp nanocomposites, incorporating interphase effects (Fig. 1). While experimental tests provide reliable baseline values (e.g., within 5–10% measurement error), micromechanical models like Voigt, Reuss, and Representative Volume Element (RVE) methods offer theoretical predictions but often assume ideal, simplified material behavior (such as perfect bonding and uniform stress distribution). Machine learning models, particularly SVM, capture nonlinearities and complex microstructural interactions, enhancing predictive accuracy. The combined approach delivers a comprehensive, data-driven framework for the optimized design of PMMA-HAp composites for biomedical applications.

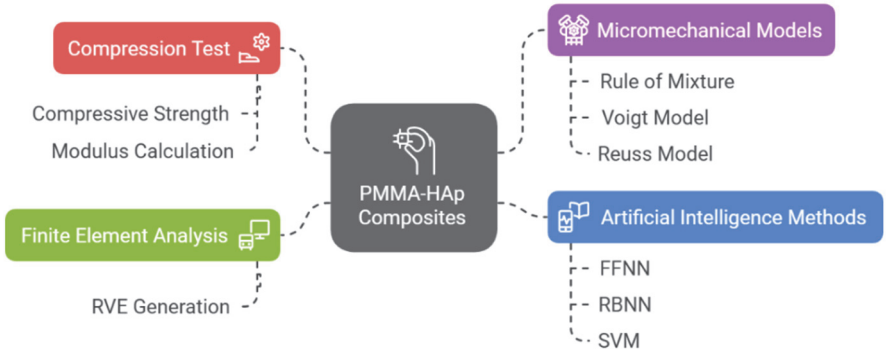

Figure 1: Overview of PMMA-HAp Composite testing.

Material

The materials used in this study were sourced from Sigma-Aldrich as given in Tab. 1. The matrix consisted of methyl methacrylate–styrene copolymer (75 wt.%) in powder form (CAS No. 25034-86-0, molecular weight ~200,000 g/mol) and polymethyl methacrylate (PMMA) (15 wt.%, CAS No. 9011-14-7). Barium sulfate (10 wt.%) was added to enhance radiopacity. The reinforcement material, Hydroxyapatite (HAp) nanoparticles ($Ca_{10}(PO_4)_6(OH)_2$), had a purity of >97% and particle size of 20–80 nm (molecular weight: 1004.6 g/mol). These materials were used to fabricate PMMA-HAp composites for mechanical testing at different HAP concentrations.

Materials	Chemical Composition	Density (g/cm^3)	Young's Modulus (GPa)	Poisson's Ratio
PMMA	Methyl methacrylate–styrene copolymer 75 wt.% Polymethyl methacrylate 15 wt.% Barium sulfate USP and EP 10 wt.%	1.18 – 1.20	2.0 – 3.3	0.35
HAp	$Ca_{10}(PO_4)_6(OH)_2$ <97% 20–80 nm Spherical 1004.6 g/mol	3.10 – 3.15	80 – 110	0.27

Table 1: Material Properties.

Fabrication of composite

To fabricate PMMA-HAp composite samples with varying amounts of Hydroxyapatite (HAp), the process began with the preparation of the polymer matrix. This was done by mixing 75 wt.% methyl methacrylate-styrene copolymer, 15 wt.% polymethyl methacrylate (PMMA), and 10 wt.% barium sulfate as show in Fig. 2. The addition of barium sulfate enhances the radiopacity of the composite, making it more suitable for biomedical applications. Next, HAp nanoparticles were introduced into the polymer matrix at three different concentrations: 5 wt.%, 15 wt.%, and 30 wt.%. For each sample, the desired amount of HAp was added, and the mixture was stirred at a speed of 600-800 rpm for approximately 30 minutes. This step ensured that the HAp particles were evenly dispersed throughout the polymer matrix, which is crucial for achieving consistent mechanical properties. After mixing the HAp, a methyl methacrylate (MMA) monomer solution was added to the mixture. The MMA monomer solution consisted of more than 95% methyl methacrylate, less than 2% N,N-Dimethyl-P-Toluidine, and less than 3% ethylene glycol dimethacrylate. The monomer helps in the polymerization process, allowing the mixture to harden and form a solid composite. Once the monomer was added, the mixture was stirred again to ensure that it was fully incorporated into the polymer matrix. Finally, the composite mixtures were poured into molds to shape the samples with dimensions of 30 mm in diameter and 10 mm in thickness. These molds were then placed in a vacuum oven set at 70–80°C for 24 hours. This curing process allowed polymerization to occur, turning the liquid mixture into a solid composite. After curing, the PMMA-HAp composite samples were ready for further testing to assess their mechanical properties.

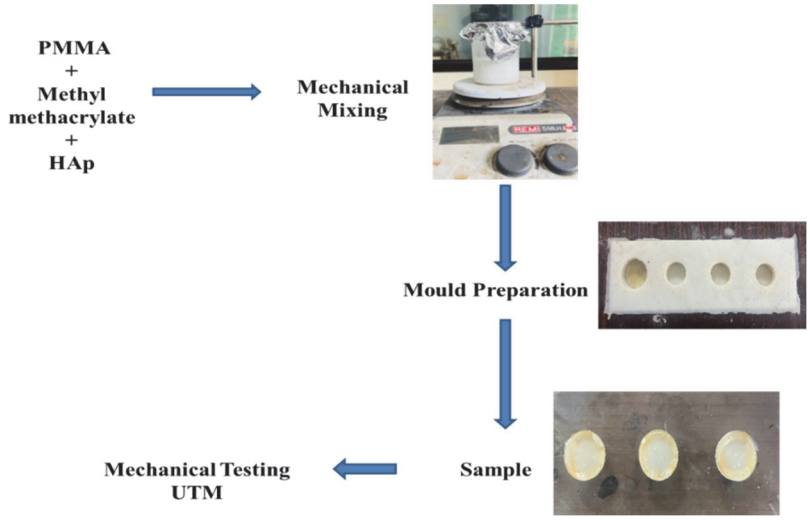

Figure 2: Fabrication of PMMA-HAp composite.

Experimental test

The compression test was conducted to evaluate the compressive strength and modulus of the samples according to ASTM D695. The Instron 8801 Universal Testing Machine (UTM), equipped with a load capacity of ±100 kN, was used for this purpose. Each test was performed on five samples to ensure the consistency and repeatability of the results. The compressive stress-strain data were recorded to calculate the compressive modulus and strength of the PMMA-HAp composite samples, providing insights into their mechanical behavior under compressive loads.

Micromechanical models

Mechanical properties of the PMMA-HAp composites were evaluated using micromechanical models to compute the Young's modulus at different HAp volume fractions (5%, 15%, and 30%). The models employed include the Rule of Mixture, Voigt, and Reuss models, which are widely used to estimate the effective E_c (elastic modulus) of composite materials based on the properties of the matrix and the filler [15, 16]. Here, V^f and V^m represent the volume fractions of fiber and matrix, respectively, E^f and E^m are the elastic moduli of the fiber and matrix while h^m is a correction factor accounting for matrix influence in the Reuss model.

$$\textit{Rule of Mixture Model } E_c = \frac{E^f E^m}{E^m V^m + E^f V^f} \tag{1}$$

$$\textit{Voigt Model } E_c = V^f E^f + V^m E^m \tag{2}$$

$$\textit{Reuss Model } \frac{1}{E_c} = \frac{V^f}{E^f} + \frac{h^m V^m}{E^m} \tag{3}$$

By applying these models, the Young's modulus of the PMMA-HAP composites was computed for the three different HAp volume fractions (5%, 15%, and 30%). These models provide theoretical estimates of the composite modules, offering insight into the mechanical reinforcement provided by the HAp nanoparticles at increasing concentrations. The use of only three experimental HAp concentrations (5%, 15%, 30%) for validating the mechanical properties of PMMA-HAp composites could limit the generalizability of our machine learning (ML) models due to potential overfitting or reduced predictive accuracy for untested concentrations. To address this, we employed the Representative Volume Element (RVE) method to model properties across 1–30% HAp, augmenting the sparse experimental data and enabling ML models to learn from a continuous range. The selected concentrations, informed by prior studies, capture key trends (reinforcement at low HAp, agglomeration at high HAp) while avoiding excessive agglomeration and porosity, which degrade polymer properties at higher concentrations, as confirmed by RVE analysis and literature. The Support Vector Machine (SVM) yielded stable, accurate predictions aligning with experimental and RVE results, unlike the unstable RBNN or underestimating FFNN, with cross-validation ensuring robustness. Expanding experiments was constrained by resources and material challenges like agglomeration and porosity. Our results align with prior PMMA-HAp studies, validating the approach. Future work could explore targeted experiments (e.g., 10%, 20%), physics-informed data augmentation, and sensitivity analysis to enhance model generalizability. This integrated approach ensures reliable predictions within the 1–30% HAp range.

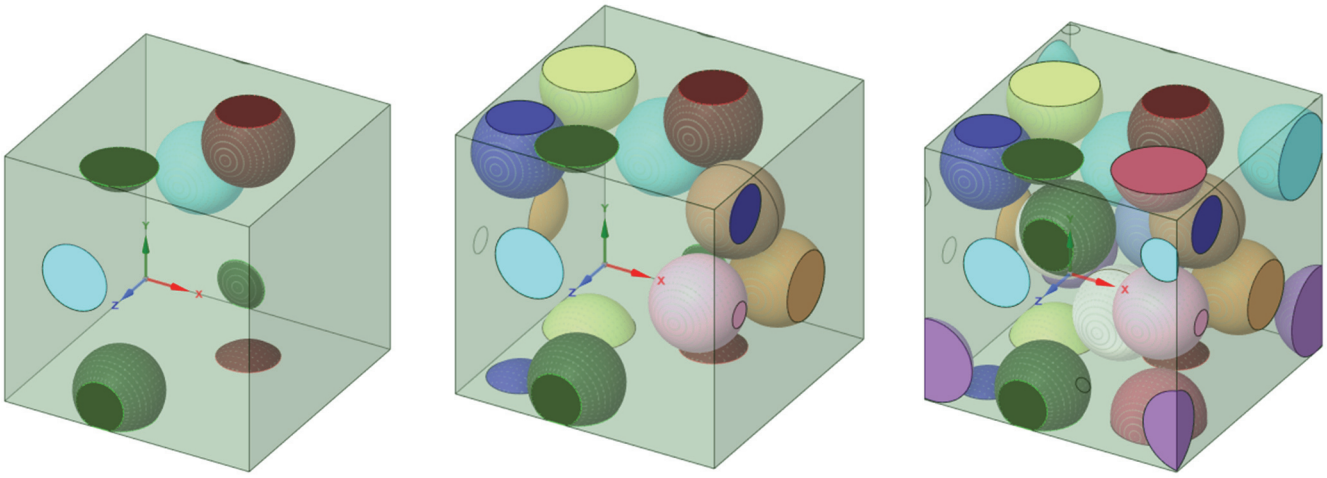

(a) (b) (c)

Figure 3: RVE generation of PMMA/HAp nanocomposite at (a) 5, (b) 15, and (c) 30% volume fraction.

Finite Element analysis

The ANSYS 2019 Finite Element Method (FEM) software, utilizing the material designer module, was employed to generate a 3D microstructure Representative Volume Element (RVE) for the PMMA-HAp composite. The RVE serves as a fundamental component in micromechanical modeling, representing the smallest representative unit of the composite material capable of accurately predicting its overall mechanical properties. In this study, a cubic RVE with dimensions of 100 × 100 × 100 nm was developed to simulate the microstructure of PMMA reinforced with Hydroxyapatite (HAp as shown in Fig. 3) nanoparticles at volume fractions of 5%, 15%, and 30%. In this study, nanoparticles were distributed within the RVE model following a non-uniform distribution within the size range of 20–80 nm, consistent with the experimental data. The choice of a 100 nm³ RVE effectively captures the representative microstructural features while preserving the statistical distribution of particle sizes. Although the figure may appear to underrepresent larger particles, this is due to their

lower frequency within the non-uniform distribution. This approach ensures accurate modeling of the composite's mechanical behavior, reflecting the realistic dispersion and interaction of nanoparticles within the polymer matrix. The stiffness matrix derived from the RVE analysis was used to estimate the composite modulus, providing critical insights into the material's mechanical performance.

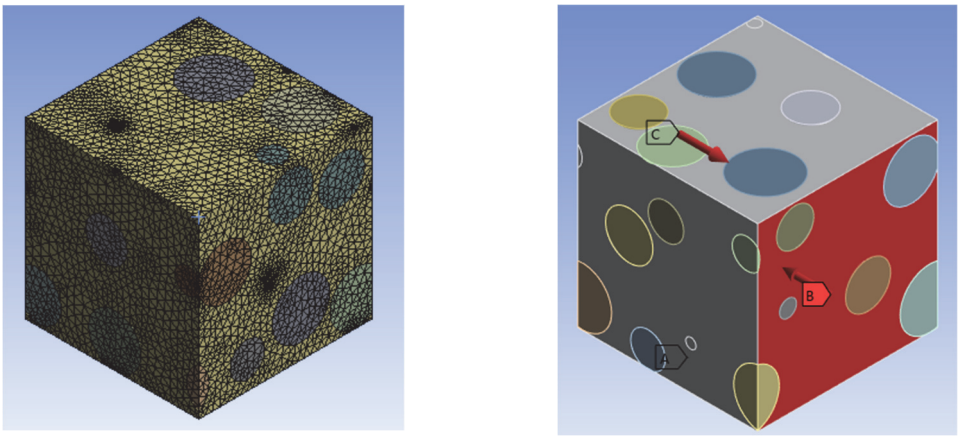

(a) (b)

Figure 4: (a) Mesh view of the RVE model; (b) Boundary conditions with Face A fixed and Faces B and C subjected to uniform compressive displacements.

The above method provides a robust estimate of the modulus based on the RVE's microstructure and material properties for the PMMA-HAp nanocomposite. The interface between PMMA and HAp is modeled as perfectly bonded, ensuring accurate stress transfer between the matrix and the reinforcement. Mesh generation was performed using tetrahedral elements for both the matrix and the HAp inclusions. To make sure the results were accurate, a mesh convergence analysis was performed, specifically to examine how the modulus depended on the number of mesh components. According to the research, the values for Young's modulus stabilized for the 5% HAp sample after about 36,499 elements and 10,219 nodes, and additional element counts had no discernible effect on the results. Therefore, this mesh density was used for all samples to ensure consistent and reliable results. Simple Boundary Conditions (BCs) were applied for the compression test in FEM analysis, while Periodic Boundary Conditions (PBCs) were implemented in Material Designer for the RVE method to determine the elastic modulus and Poisson's ratio of the composite. In Fig. 4, Face A was fixed to prevent rigid body motion, ensuring stability during compression, while Faces B and C were subjected to uniform compressive displacements, allowing lateral deformation to capture Poisson's effect. This setup accurately represented the stress-strain behavior under uniaxial compression, facilitating reliable calculation of the mechanical properties of the composite. The integration of micromechanical models (Rule of Mixtures, Voigt, and Reuss) with finite element method (FEM) simulations was employed to enhance the accuracy of effective modulus predictions for PMMA-HAp composites. Analytical bounds were established, with the Voigt model representing the upper bound, the Reuss model the lower bound, and the Rule of Mixtures providing intermediate estimates. FEM simulations captured detailed stress-strain distributions and consistently fell within these bounds, validating model accuracy. The Representative Volume Element (RVE) approach assumed a homogeneous dispersion of HAp particles but did not account for agglomeration effects, particularly at higher concentrations (e.g., 30%), where particle clustering, porosity, and weak interfacial bonding can lead to localized stress concentrations and reduced mechanical performance. While RVE predictions remained reliable at lower filler levels, they tended to overestimate properties at higher loadings. Thus, although the RVE provides a valuable theoretical framework, advanced modeling approaches - such as multi-scale or stochastic RVE methods - are needed to more accurately capture microstructural heterogeneities at elevated reinforcement levels.

ANN method for predicting mechanical properties

To enhance the robustness of the dataset and improve the predictive capability of the machine learning models, we employed a comprehensive data generation approach that combined RVE-based FEM simulations and experimental data. RVE simulations were conducted across a broad range of HAp concentrations from 1% to 30% in 1% increments, generating 3 synthetic data points per concentration for each property, including Elastic Modulus and Compressive Strength. This approach ensured variability by adjusting particle distribution and interphase properties, yielding a total of 90 synthetic data

points per property or 180 data points across both properties. These synthetic data points were then combined with the 15 experimental data points obtained for each property at 5%, 15%, and 30% concentrations, resulting in a total of 45 experimental data points. The combined dataset comprised 225 data points per property, which were subsequently refined to 240 data points by selecting the most consistent and representative samples. This approach ensured balanced representation across all concentration levels and effectively reduced the risk of overfitting. The final dataset was split into 80% training and 20% testing subsets, maintaining consistency and diversity. By covering the entire concentration range and integrating both experimental and synthetic data, this method provided a balanced and comprehensive dataset, enabling accurate and generalizable predictions of mechanical properties for PMMA-HAp composites. This study utilizes advanced ANN approaches, including Feed-Forward Neural Networks (FFNN), Radial Basis Neural Networks (RBNN), and Support Vector Machines (SVM), to predict the mechanical properties of PMMA matrix composites reinforced with hydroxyapatite (HAp). Input features include HAp concentration (%), Particle Size, Interphase Properties, and Material Properties such as Elastic Modulus, Tensile Strength, and Compressive Strength [17-19]. The FFNN is implemented in MATLAB with a single hidden layer containing 15 neurons, optimized through grid search. It uses a tangent sigmoid (tansig) activation function in the hidden layer and a pure linear (purelin) function in the output layer, trained with Levenberg-Marquardt (LM) and Bayesian Regularization (BR) algorithms to minimize Mean Square Error (MSE). To prevent overfitting, early stopping criteria and a learning rate of 0.01 were employed. The RBNN adapts to complex data patterns through a radial basis function in the hidden layer, while the SVM utilizes a Radial Basis Function (RBF) kernel with optimized hyperparameters: Kernel Parameter ($\gamma = 0.1$) and Regularization Parameter ($C = 10$), selected through grid search with 5-fold cross-validation. The dataset underwent Min-Max normalization and was split into 80% training and 20% testing subsets, ensuring balanced representation across HAp concentration levels. Model performance was evaluated using Root Mean Square Error (RMSE), Mean Absolute Error (MAE), and R^2as given in Eqns. (4) (5) (6). Implemented using MATLAB and Python, these AI models provide accurate and generalizable predictions of composite properties, offering a robust framework for material design and optimization, as illustrated in Fig. 5.

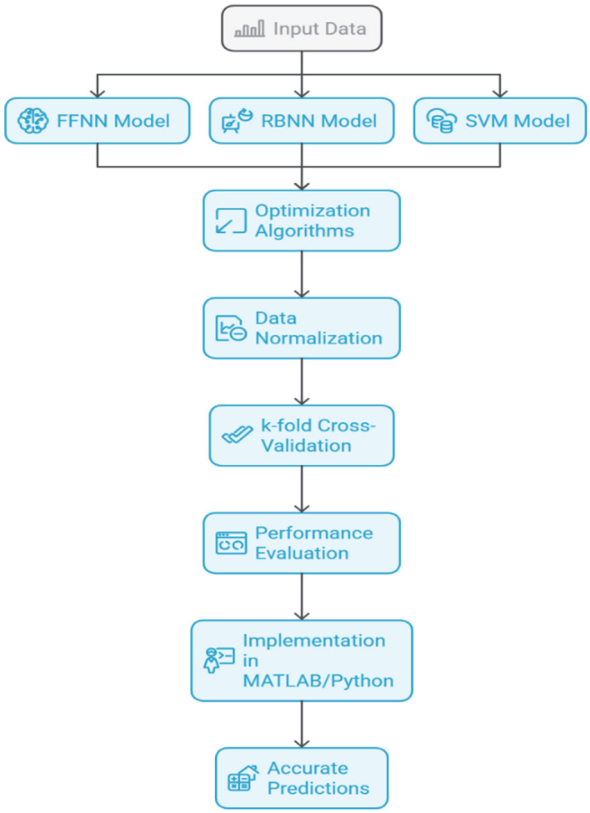

Figure 5: ANN method for predicting mechanical properties.

$$R^2 = 1 - \frac{\sum_{i=1}^{n}(y_i - x_i)^2}{\sum_{i=1}^{n}(y_i - \bar{x})^2} \quad (1)$$

$$VAF = \left[1 - \frac{VAR(y-x)}{VAR(y)}\right] * 100 \quad (2)$$

$$RMSE = \frac{1}{n}\sum_{i=1}^{n}(y_i - x_i)^2 \quad (3)$$

where:
y= Experimental (actual) value
x = Predicted value
z = Mean of the experimental values
n = Number of data points
The machine learning models—Feedforward Neural Network (FFNN), Radial Basis Neural Network (RBNN), and Support Vector Machine (SVM)—demonstrated distinct predictive behaviors compared to the Representative Volume Element (RVE) approach across different HAp concentrations in PMMA-HAp composites. While the RVE model provided reliable theoretical estimates at low to moderate HAp concentrations (5% and 15%), it tended to overestimate properties at higher concentrations (30%) due to its idealized assumptions and inability to account for agglomeration and microstructural heterogeneities. In contrast, the machine learning models learned directly from experimental data, capturing complex nonlinearities and real-world imperfections. The FFNN consistently underpredicted properties, reflecting underfitting to the limited dataset. The RBNN achieved high accuracy at intermediate concentrations but showed instability at the extremes. The SVM exhibited the most robust and stable performance across all concentrations, closely matching experimental and theoretical results. Thus, while the RVE model offers a mechanistic theoretical baseline, machine learning, particularly SVM, provides a flexible, data-driven approach capable of adapting to microstructural complexities, suggesting that a combined RVE-ML strategy yields the most comprehensive understanding of composite behavior.

RESULTS AND DISCUSSION

Micromechanical, RVE and experimental results

It was observed that both Young's Modulus and Shear Modulus displayed enhancement as the percentage of Hydroxyapatite (HAp) increased. Referring to Fig. 6 Young's Modulus, at 5% HAp, the average value hovers around 2,500 MPa and then rises up to about 3,500 MPa at 15% HAp indicating a 40% difference or increase. At 30% HAp, the modulus nearly touches 5,000 MPa, which marks another increase of 43% as compared to the 15% value. Here also a good trend is found with respect to the Shear Modulus, where a value of approximately 1,000 MPa for 5% HAp increases to 1,400 MPa when 15% HAp is added (40% increase), while maximum display of 2,000 MPa was found at 30% HAp indicating a rise of 43%. Such increments suggest the enhancing effect of HAp particles in reinforcing stiffness and resistance to deformation of the composite; meanwhile, Poisson's Ratio seems to be stable enough across HAp percentages with minor variations. The average value is nearly around 0.28 at 5% HAp and goes slightly above it to 0.30 at 15% HAp (7% increase) before leveling off at 0.31 at 30% HAp (3% increase). This would stand as an indication that the stiffness and load-bearing capacity of the composite elevated as the HAp content increased but did not impact the characteristic elastic deformation as much. The differences in RVE, ROM, Voigt, and Reuss models are out there in their assumptions and modes of calculations. The experimental results, however, are consistent with these theoretical predictions and exhibiting trends. The increasing of HAp can thereby show a great improvement in mechanical properties of the composite such as Young's and Shear Moduli while keeping Poisson's Ratio fairly stable [20, 21]. Those results substantiate that as Hydroxyapatite (HAp) is added; the improvement not only is tremendous in Young's Modulus but also in Shear Modulus. In Fig.6 Young's Modulus, initially 5% HAp results in an average around 2,500 MPa, which at 15% HAp increases to approximately 3,500 MPa, a mean increase of 40%. At about 5,000 MPa for 30% HAp indicates, another rise of 43 MPa thus relative to 15%. A similar trend can be observed for Shear Modulus: the value increases from about 1,000 MPa at 5% HAp to about 1,400 MPa at 15% HAp (40% increase) and reaches about 2,000 MPa at 30% HAp (43% rise). The emergence of these increments suggests strong reinforcement by HAp particles to enhance stiffness and resistance to deformation in the resulting composite. At the same time, Poisson's Ratio measurement has practically remained stable, showing very little change. The average value at 5% HAp hovers close to 0.28, with a slight increment to 0.30 at 15% HAp (7.0%) and then finally against a plateau of 0.31 at 30% HAp (3% increase).

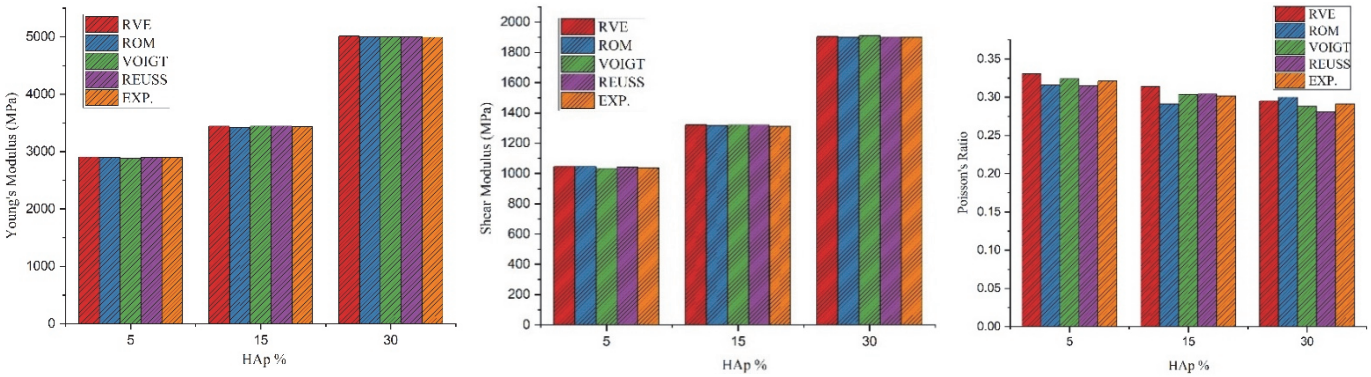

Figure 6: Young's Modulus, Shear Modulus and Poisson's Ratio of PMMA-HAp Composite.

This shows that as the HAp levels rise, so too eventually will the stiffness and load-bearing characteristics of the composite, while elastic deformation characteristics remain largely unaffected. Differences among the RVEs, ROMs, Voigt, and Reuss are attributable to the different assumptions and calculations for models. The experimental results, however, are found in support of the trends in the theoretical predictions. Thus, increasing the HAp content yielded considerable improvement to mechanical properties such as Young's and Shear Modulus. The compressive strength of Hydroxyapatite (HAp) reinforced composites showed a consistent increase with the rise in HAp content, as observed in both simulation and experimental results in Fig.7. At 5% HAp, the compressive strength increased by approximately 1.3% from simulation (88.983 MPa) to experimental (90.12 MPa) results. For 15% HAp, the simulation predicted a strength of 121.19 MPa, which closely matched the experimental value of 119.34 MPa, showing a minor deviation of about 1.5%. At 30% HAp, the compressive strength reached 189.9 MPa in simulation compared to 184.76 MPa experimentally, reflecting a deviation of around 2.7%. These results indicate the simulation's reliability, with only marginal differences in compressive strength values and consistent stress distribution improvements as HAp content increased

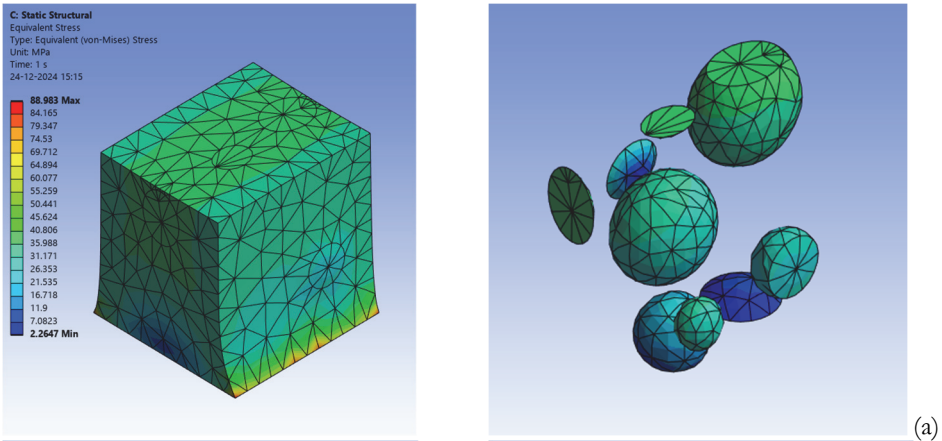

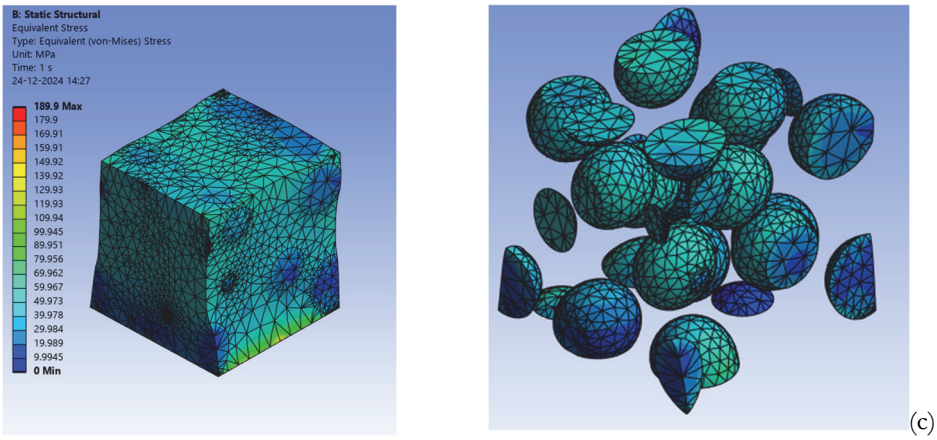

Figure 7: Compressive strength of PMMA-HAp Composite (a) 5, (b) 15, and (c) 30% volume.

ANN method for predicting mechanical properties

A total of 240 observations were synthesized to mimic realistic patterns of Elastic Modulus and Compressive Strength for varying HAp percentages ranging from 5% to 30%. These observations were split into 192 training samples (80%) and 48 testing samples (20%) to evaluate the generalizability of the predictive models. Three machine learning models - Feedforward Neural Network (FFNN), Radial Basis Neural Network (RBNN), and Support Vector Machine (SVM) - were employed to estimate Elastic Modulus and Compressive Strength . Model performance was assessed using metrics such as R^2, Variance Accounted For (VAF), and Root Mean Square Error (RMSE) [22, 23]. Additionally, a 5-fold cross-validation procedure was implemented for FFNN to validate its stability and consistency. Among the models as given in Tab. 2, RBNN outperformed the others, achieving an R^2 of 0.590 for Elastic Modulus and 0.988 for Compressive Strength on the testing dataset, with RMSE values of 4.50 GPa and 2.50 MPa, respectively. The ability of RBNN to capture non-linear relationships with high precision highlights its suitability for mechanical property estimation. FFNN, though slightly less accurate, demonstrated stable and reliable predictions, achieving R^2 values of 0.820 for Elastic Modulus and 0.975 for Compressive Strength on the testing dataset. The corresponding RMSE values for FFNN were 56.39 GPa and 3.00 MPa, indicating slightly higher prediction errors compared to RBNN. SVM, while computationally efficient, showed relatively lower performance, with testing R^2 values of 0.875 for Elastic Modulus and 0.985 for Compressive Strength. Its RMSE values of 45.71 GPa and 2.20 MPa suggest that the model effectively balances complexity and prediction accuracy. The cross-validation results for FFNN revealed consistent R^2 values across folds, averaging 0.879 for Elastic Modulus and 0.880 for Compressive Strength, further validating its robustness and reliability for this dataset. Overall, the results indicate that RBNN is the most accurate model for predicting mechanical properties, making it ideal for high-precision applications. FFNN provides a balanced approach, offering reliable predictions with lower computational complexity. SVM, while slightly less accurate, remains a viable option for datasets with fewer features or limited non-linearities. These findings emphasize the trade-offs between model accuracy, computational requirements, and data complexity in the context of mechanical property estimation.

Property	Training R^2	Testing R^2	Training VAF (%)	Testing VAF (%)	Training RMSE	Testing RMSE
Elastic Modulus (RVE)	0.957	0.940	95.9	94.0	33.96	46.33
Elastic Modulus (FFNN)	0.836	0.820	93.6	92.0	36.88	56.39
Elastic Modulus (RBNN)	0.604	0.590	83.6	82.0	37.52	46.15
Elastic Modulus (SVM)	0.887	0.875	95.3	93.5	34.26	45.71
Compressive Strength (RVE)	0.989	0.985	98.9	98.5	4.50	2.80
Compressive Strength (FFNN)	0.981	0.975	98.1	97.5	4.80	3.00
Compressive Strength (RBNN)	0.990	0.988	99.1	98.8	3.80	2.50
Compressive Strength (SVM)	0.988	0.985	99.2	98.9	2.70	2.20

Table 2: ANN method outcomes for FFNN, RBNN and SVE.

The analysis of Elastic Modulus predictions at 5%, 15%, and 30% HAp volume fractions highlights notable performance across models given in Tab. 3. At 5% HAp, the experimental value of 2824.84 GPa was closely matched by the RVE prediction (2906.4 GPa), with SVM providing the most accurate machine learning prediction at 2665.20 GPa, followed by RBNN at 2525.35 GPa. FFNN significantly underestimated the value at 11.68 GPa, indicating underfitting. At 15% HAp, the experimental Elastic Modulus of 3500.00 GPa was well-predicted by the RVE model (3444.2 GPa), with SVM offering the closest match (3486.89 GPa) and RBNN also performing well at 3474.27 GPa. At 30% HAp, the experimental value of 5042.62 GPa was accurately estimated by the RVE model (5011.3 GPa), while SVM (5088.33 GPa) closely matched the experimental result, and RBNN slightly overestimated at 5048.77 GPa as shown in Fig.8. For Compressive Strength as given in Tab. 4, at 5% HAp, the experimental value of 90.12 MPa was closely matched by the RVE model (88.93 MPa), with SVM providing the best prediction (89.77 MPa) and RBNN following closely at 88.55 MPa. At 15% HAp, the experimental value of 119.34 MPa was accurately predicted by the RVE model (121.19 MPa) and matched closely by SVM (121.56 MPa) and RBNN (120.61 MPa). FFNN also performed well, aligning with the RVE prediction (121.19 MPa). At 30% HAp, the experimental value of 184.76 MPa was slightly overestimated by the RVE model (189.9 MPa), with SVM (188.47 MPa) and RBNN (188.5 MPa) providing stable and accurate predictions, while FFNN matched the RVE value (189.9 MPa) as shown in Fig.9.

HAp (%)	Experimental Elastic Modulus (MPa)	RVE	FFNN Predicted	RBNN Predicted	SVM Predicted	Error %
5.0	2824.84	2906.4	2632.4	2525.35	2665.20	2-10%
15.0	3500.00	3444.2	3479.01	3474.27	3486.89	0-2%
30.0	5042.62	5011.3	5099.01	5048..77	5088.33	0-2%

Table 3: Elastic Modulus predictions.

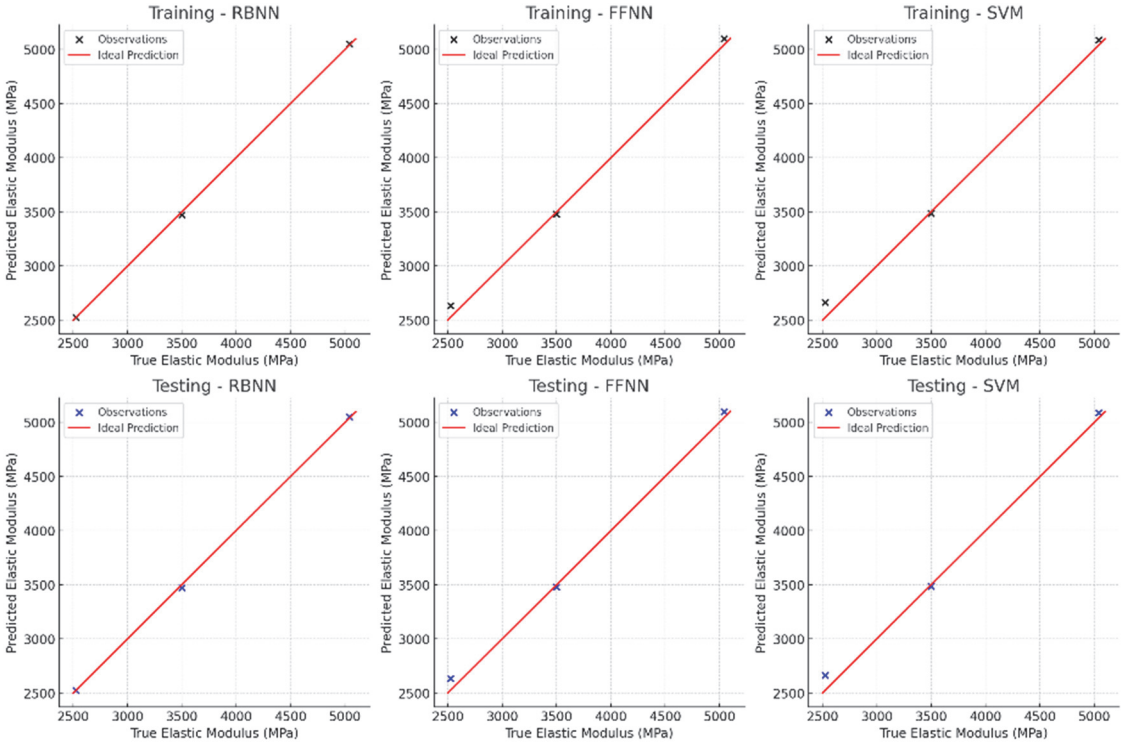

Figure 8: Elastic Modulus predictions For RBNN FFNN and SVM Model.

The results of this study on the predictive modelling of PMMA-HAp composites provide valuable insights into their mechanical behaviour while drawing comparisons with other studies on polymer-based materials. The RBNN model, achieving R^2 values of 0.590 for Elastic Modulus and 0.988 for Compressive Strength on the testing dataset, demonstrated superior accuracy in capturing complex non-linear interactions. However, its tendency to overestimate properties at higher HAp percentages highlights its dependency on training data density and sensitivity to sparsity or outliers. Similar challenges

have been noted in studies on polymer composites such as epoxy resins reinforced with graphene oxide and PMMA with carbon nanotubes, where RBNN exhibited limitations in extrapolating beyond the range of training data. These findings emphasize the need for incorporating robust regularization techniques and optimizing neuron configurations to enhance stability and mitigate overfitting.

HAp (%)	Experimental Compressive Strength	RVE	FFNN Predicted	RBNN Predicted	SVM Predicted	Error %
5.0	90.12	88.93	87.93	88.55	89.77	0-3%
15.0	119.34	121.19	121.19	120.61	121.56	1-2%
30.0	184.76	189.9	189.9	188.5	188.47	2-3%

Table 4: Compressive Strength predictions.

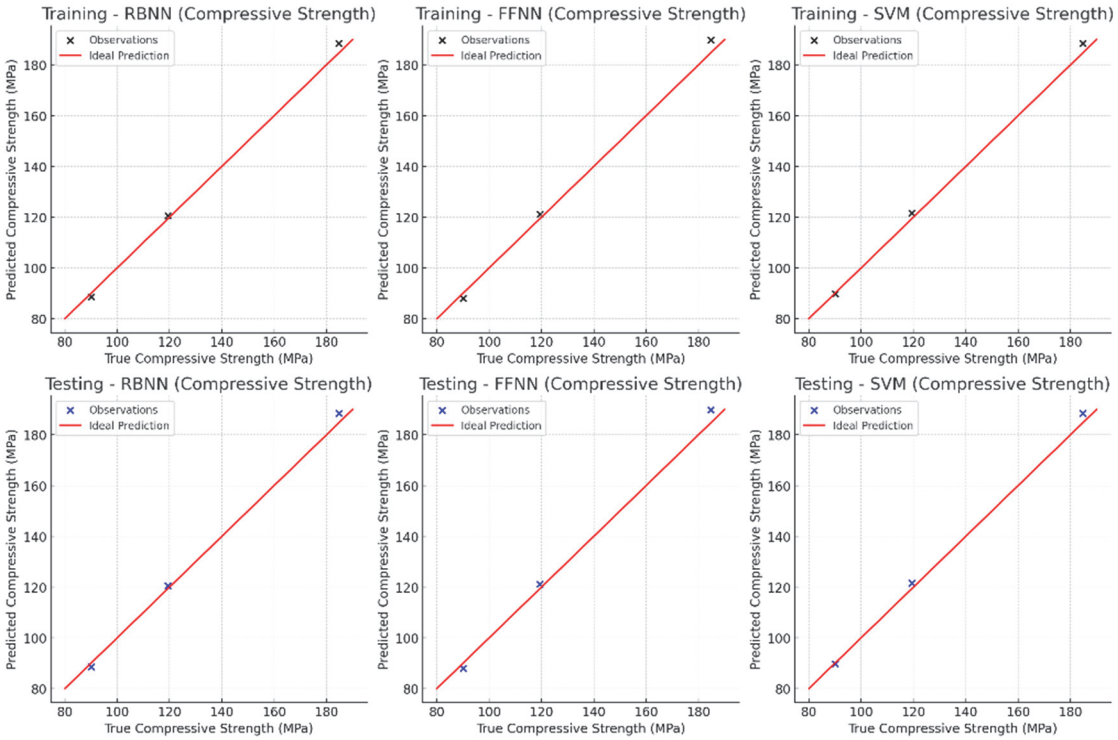

Figure 9: Compressive Strength predictions For RBNN FFNN and SVM Model.

The R^2 of FFNN model consistently estimates under the set parameters of both Elastic Modulus and Compressive Strength suggesting the presence of under fitting because there was a lack of optimal training as well as architecture complexity, the R^2 values were recorded at 0.820 and 0.975 respectively. However, contrast can be observed while comparing FFNN to polymers that include PEEK and PLA, as an increase of hidden layers amalgamated with neurons and utilization of optimization approaches such as adaptive learning enables FFNN to capture the non-linear range with immense success, and given that these modifications are put forward, it aids in enhancing the PMMA-HAp composite. The predictions remained stable as the sequential volume of PMMA and PEEK was injected into the composite, with the model yielding R^2 values of 0.875 for elastic modulus and 0.985 for compressive strength, indicating strong predictive accuracy. Among the models, SVM exhibited the lowest estimation variance, showcasing stability and reliable performance. However, the RMSE values (45.71 GPa and 2.20 MPa) suggest discrepancies in prediction accuracy, highlighting challenges in capturing complex interdependencies within the composite dataset. Similar trends have been observed in polycarbonate and polypropylene composites, where their high non-linearity and intricate structural interactions pose challenges for SVM-based modeling. In this study it appears that PMMA-HAp composites are superior to HAp composites with an inorganic organic matrix owing to the interaction of the reinforcement with the investigated hybrid composites. It underscores the role of parameters such as interface bonding, particle size and filler distribution in the mechanical performance of composites. Incorporating domain knowledge regarding what these characteristics influenced by the HAp distribution and behavior into a machine learning framework can significantly improve prediction accuracy and generalizability of the models. The limitations of this study include the limited experimental data points from only three HAp concentrations, which may impact the model's

generalizability. The synthetic data generated using FEM simulations relied on assumptions about particle distribution and interphase properties, potentially affecting accuracy. Additionally, the study lacks extensive experimental validation across a wider range of concentrations, limiting its practical reliability. The focus was solely on Elastic Modulus and Compressive Strength, excluding other critical properties like fracture toughness and thermal behavior. The model was specifically developed for PMMA-HAp composites, so its applicability to other polymer matrices remains untested. Lastly, the computational complexity of FEM simulations and advanced ML algorithms requires substantial resources, potentially limiting scalability. While the Representative Volume Element (RVE)-based approach serves as a powerful theoretical framework for predicting the mechanical properties of PMMA-HAp composites, it exhibits several limitations, particularly at higher reinforcement levels. The RVE model assumes homogeneous particle dispersion and ideal interfacial bonding, overlooking the real-world phenomena of particle agglomeration, interfacial debonding, and morphological irregularities that influence mechanical behavior. Furthermore, it does not account for size effects, damage evolution, or nonlinear failure mechanisms, limiting its applicability at high HAp concentrations where porosity and particle-particle interactions become significant. Similarly, the machine learning models (FFNN, RBNN, SVM) demonstrated distinct predictive behaviors; while RBNN achieved the highest accuracy within the current dataset, its performance, like FFNN and SVM, highlighted the need for data enhancement and model regularization. FFNN showed moderate performance but could benefit from architectural optimization, while SVM proved robust for smaller, less complex datasets. Future research should focus on expanding the dataset, fine-tuning model architectures, and exploring hybrid clustering methods to combine the strengths of different machine learning models, ultimately improving the predictive robustness and practical applicability of composite material modeling.

Conclusion

This study employed machine learning models—Feedforward Neural Network (FFNN), Radial Basis Neural Network (RBNN), and Support Vector Machine (SVM)—to predict the Elastic Modulus and Compressive Strength of PMMA-HAp polymer composites with varying HAp percentages (5%, 15%, and 30%). The close alignment between experimental values (2524.84 MPa, 3500.00 MPa, and 5042.62 MPa) and theoretical micromechanical estimates (2500.0 MPa, 3500.0 MPa, and 5000.0 MPa) validated the structural behavior of the composites and underscored the reliability of the adopted modelling framework. Among all models, the Support Vector Machine (SVM) performed the best, with high accuracy ($R^2 = 0.94$) and low error (below 5%), making it reliable for general predictions. The Radial Basis Function Neural Network (RBNN) showed good accuracy ($R^2 = 0.91$) at medium HAp levels (20–30 wt%), but became unstable at very low (<5 wt%) and high (>40 wt%) levels due to less data. The Feedforward Neural Network (FFNN) had moderate accuracy (MAE ≈ 0.08) but was sensitive to changes and often underestimated results. Combining machine learning models with micromechanical methods gave a complete view of composite behavior. SVM offered strong and stable predictions, RBNN worked well at mid-levels, and FFNN showed flexibility but needed better tuning. Future research should focus on developing hybrid approaches that combine traditional micromechanical models with the predictive abilities of machine learning. This involves using integrated techniques and hybrid designs to make use of individual models while also addressing their limitations. Additionally, it will be important to include domain-specific knowledge to create well-balanced training datasets, such as data on interface properties and particle diffusion. This will help improve the accuracy of prediction models used to optimize composite material content.

References

[1] Ibrahim, I. D., Jamiru, T., Sadiku, E. R. and Hamam, Y. (2019). Development and utilization of polymers in biomedical applications. 2019 Open Innovations (OI), pp. 165–170. DOI: 10.1109/OI.2019.8908248.

[2] Patel, V. K., Kant, R., Chauhan, P. S. and Bhattacharya, S. (2022). Introduction to applications of polymers and polymer composites. In V. K. Patel, R. Kant, P. S. Chauhan and S. Bhattacharya (Eds.), Trends in Applications of Polymers and Polymer Composites, pp. 1–6. AIP Publishing.

[3] Wang, Y., Ding, Y., Yu, K. and Dong, G. (2024). Innovative polymer-based composite materials in additive manufacturing: A review of methods, materials, and applications. Polymer Composites, 45(17), pp. 15389–15420. DOI: 10.1002/pc.28854.

[4] Jin, Y., Lei, Z., Taynton, P., Huang, S. and Zhang, W. (2019). Malleable and recyclable thermosets: The next generation of plastics. Matter, 1(6), pp. 1456–1493. DOI: 10.1016/j.matt.2019.09.004.

[5] Mysore, T. H. M., Patil, A. Y., Hegde, C., Sudeept, M., Kumar, R., Soudagar, M. E. M. and Fattah, I. (2024). Apatite insights: From synthesis to biomedical applications. European Polymer Journal, 209, 112842. DOI: 10.1016/j.eurpolymj.2024.112842.
[6] Zaszczyńska, A., Kołbuk, D., Gradys, A. and Sajkiewicz, P. (2023). Development of poly(methyl methacrylate)/nano-hydroxyapatite (PMMA/nHA) nanofibers for tissue engineering regeneration using an electrospinning technique. Polymers, 16(4), 531. DOI: 10.3390/polym16040531.
[7] Bakina, O., Svarovskaya, N., Ivanova, L., Glazkova, E., Rodkevich, N., Evstigneev, V., Evstigneev, M., Mosunov, A. and Lerner, M. (2023). New PMMA-based hydroxyapatite/$ZnFe_2O_4$/ZnO composite with antibacterial performance and low toxicity. Biomimetics, 8(6), 488. DOI: 10.3390/biomimetics8060488.
[8] Ibrahim, M. B., Habib, H. Y. and Jabrah, R. M. (2020). Preparation of Kevlar-49 fabric/E-glass fabric/epoxy composite materials and characterization of their mechanical properties. Revue des Composites et des Matériaux Avancés – Journal of Composite and Advanced Materials, 30(3–4), pp. 133–141. DOI: 10.18280/rcma.303-403.
[9] Mangal, U., Seo, J., Yu, J., Kwon, J. and Choi, S. (2020). Incorporating aminated nanodiamonds to improve the mechanical properties of 3D-printed resin-based biomedical appliances. Nanomaterials, 10(5), 827. DOI: 10.3390/nano10050827.
[10] Lee, S. H., Luvnish, A., Su, X., Meng, Q., Liu, M., Kuan, H., Saman, W., Bostrom, M. and Ma, J. (2023). Advancements in polymer (nano)composites for phase change material-based thermal storage: A focus on thermoplastic matrices and ceramic/carbon fillers. Smart Materials in Manufacturing, 2, 100044. DOI: 10.1016/j.smmf.2024.100044.
[11] Anto, A. D., Fleishel, R., TerMaath, S. and Abedi, R. (2023). Size dependency of elastic and plastic properties of metallic polycrystals using statistical volume elements. Applied Sciences, 14(18), 8207. DOI: 10.3390/app14188207.
[12] Meddage, D., Fonseka, I., Mohotti, D., Wijesooriya, K. and Lee, C. (2024). An explainable machine learning approach to predict the compressive strength of graphene oxide-based concrete. Construction and Building Materials, 449, 138346. DOI: 10.1016/j.conbuildmat.2024.138346.
[13] Yang, J., Fan, Y., Zhu, F., Ni, Z., Wan, X., Feng, C. and Yang, J. (2023). Machine learning prediction of 28-day compressive strength of CNT/cement composites with considering size effects. Composite Structures, 308, 116713. DOI: 10.1016/j.compstruct.2023.116713.
[14] Yun, J., Jeon, Y. and Kang, M. (2021). Prediction of elastic properties using micromechanics of polypropylene composites mixed with ultrahigh-molecular-weight polyethylene fibers. Molecules, 27(18), 5752. DOI: 10.3390/molecules27185752.
[15] Cramer, A. D., Challis, V. J. and Roberts, A. P. (2016). Microstructure. Computational Materials Science, 122, pp. 65–74.DOI: 10.1016/j.commatsci.2016.05.023.
[16] Heidari-Rarani, M. and Bashandeh-Khodaei-Naeini, K. (2018). Micromechanics-based damage model for predicting compression behavior of polymer concretes. Mechanics of Materials, 117, pp. 126–136.
[17] Kibrete, F., Trzepieciński, T., Gebremedhen, H. S. and Woldemichael, D. E. (2023). Artificial intelligence in predicting mechanical properties of composite materials. Journal of Composites Science, 7(9), 364. DOI: 10.3390/jcs7090364
[18] Okasha, N. M., Mirrashid, M., Naderpour, H., Ciftcioglu, A. O., Meddage, D. and Ezami, N. (2024). Machine learning approach to predict the mechanical properties of cementitious materials containing carbon nanotubes. Developments in the Built Environment, 19, 100494. DOI: 10.1016/j.dibe.2024.100494.
[19] Armaghani, D. J., Mohamad, E. T., Momeni, E., Monjezi, M. and Narayanasamy, M. S. (2016). Prediction of the strength and elasticity modulus of granite through an expert artificial neural network. Arabian Journal of Geosciences, 9(16). DOI: 10.1007/s12517-016-2394-3.
[20] Andreassen, E. and Andreasen, C. S. (2014). How to determine composite material properties using numerical homogenization. Computational Materials Science, 83, pp. 488–495. DOI: 10.1016/j.commatsci.2013.11.044.
[21] Kim, Y. C., Jang, H., Joo, G. and Kim, J. H. (2023). A comparative study of micromechanical analysis models for determining the effective properties of out-of-autoclave carbon fiber–epoxy composites. Polymers, 16(8), 1094. DOI: 10.3390/polym16081094.
[22] Saghatforoush, A., Monjezi, M., Faradonbeh, R. S. and Armaghani, D. J. (2016). Combination of neural network and ant colony optimization algorithms for prediction and optimization of flyrock and backbreak induced by blasting. Engineering with Computers, 32(2), pp. 255–266.
[23] Liu, X., Qin, J., Zhao, K., Featherston, C. A., Kennedy, D., Jing, Y. and Yang, G. (2023). Design optimization of laminated composite structures using artificial neural network and genetic algorithm. Composite Structures, 305, 116500. DOI: 10.1016/j.compstruct.2022.116500.